A microscopic method for the evaluating of continuous pedestrian dynamic models

Zhongyi Huang[a], Mohcine Chraibi[b], Shuchao Cao[c], Chuanli Huang[a], Zhiming Fang[d], Weiguo Song[a,*]

[a]*State key Laboratory of Fire Science, University of Science and Technology of China, Hefei 230027, China*
[b]*Institute for Advanced Simulation, Forschungszentrum Jülich, Jülich 52425, Germany*
[c] *School of Automotive and Traffic Engineering, Jiangsu University, Zhenjiang 212013, China*
[d]*Business School, University of Shanghai for Science and Technology, Shanghai 200093, China*

Abstract

In this paper, we propose a microscopic method to evaluate continuous pedestrian dynamic models at the trajectory level. By comparing the experimental and the simulated trajectory in four directions, the evaluation of the model can be described by a radar chart, with which both qualitative and quantitative conclusions can be obtained. In order to demonstrate our method, we evaluate a social force model by 1,936 trajectories with graded densities in three different scenarios. Three qualitative conclusions are obtained by observing radar charts of the simulation of the unidirectional experiments. All of them are verified by the comparison of the macroscopic parameters. Besides, we find that a model with smaller error in our method always has a better performance at the macroscopic level. At last, the possible quantitative descriptions of the method are discussed. Compared to the evaluations by comparing collective features like fundamental diagram, our method is general, comprehensive and quantitative. The method provides a new possibility to evaluate any continuous pedestrian dynamic model in any scenario with a standard process.

Keywords: Pedestrian dynamics, social force model, evaluation, trajectory, radar chart, validation

1. Introduction

The modeling of pedestrian movements has been a hot topic in the past decades for its wide application in architecture [1], safety engineering [2, 3], urban planning [4], robotics and animation [5]. A large number of models, such as cellular automata (CA) [6, 7, 8], force-based models [9, 10, 11], velocity based models [12], Goal-oriented models [13, 14, 15], and the optimal step model (OSM) [16, 17] have been developed. To make the models more realistic, calibrating and validating processes are necessary before applying the modeling results into practice.

*Corresponding author
Email address: wgsong@ustc.edu.cn (Weiguo Song)

In the process of calibrating and validating, a generalized evaluating method and a diverse experimental database are important. In this paper, we divide the existing evaluating methods into macroscopic and microscopic with respect to the level of the data they use. Collective characteristics such as flow rate [18, 19], movement time [20], the relation between velocity and density (known as fundamental diagram) [11] or their combinations [21] are often used in the macroscopic methods. Macroscopic methods are straightforward, for the reason that some characteristics are the main focus for the application of the model. Besides, there are some well-know collective benchmarks [22, 23]. Nevertheless, there are some common problems in the macroscopic methods. At fist, macroscopic evaluating methods are always qualitative, which is a barrier when a comparison between different models has to be made. In [24], the shape of the curve plotted from pedestrian number inside the corridor as a function of time is compared between simulations and experiments. In [21], experimental and simulation trajectories are compared by the overlap of the trajectories. Although from these comparisons it is possible to draw some conclusions with respect to experimental data, it is however difficult to perform evaluations and ratings when a lot of models, which have different shapes of curves and distributions of trajectories, have to be compared with each other. Secondly, the applicability of the macroscopic methods in different scenarios is limited and can be scenario specific. For example, the movement time is always used in the bottleneck scenario, while it could be meaningless when describing pedestrian movements in a corridor. Finally, it is possible that a model has considerable accuracy when evaluated with a macroscopic feature while has big error when evaluated with another feature. This phenomenon has been described in [21], in which the simulation flow matches the experimental flow well by adjusting parameters, while the time series of density still show obvious discrepancies with respect to experiments. The reason is summarized as that the coincident flow through bottleneck is actually achieved by the discrepant density and velocity [21].

The microscopic method is usually defined at the trajectory level. Simulating the movement of one pedestrian with a spacial continuous model while the other pedestrians are moving according to the experimental trajectories, we can get a simulated trajectory of a specific participant. In [25, 26], error (e) is defined based on acceleration difference between simulated and experimental trajectories:

$$e = \sum_{i} \sum_{t=t_i^{start}}^{t_i^{end}} [(\tilde{f}_i^x(t) - f_i^x(t))^2 + (\tilde{f}_i^y(t) - f_i^y(t))^2], \tag{1}$$

where i is a pedestrian, t is the time stamp, $[\tilde{f}_i^x(t), \tilde{f}_i^y(t)]$ is the acceleration at time t obtained from experimental trajectory, and $[f_i^x(t), f_i^y(t)]$ is the acceleration simulated by a social-force-based model at time t. According to the definition, the comparison is based on the second derivation of a trajectory. This method has been criticized by the authors of Ref. [25] themselves in their another work [27], in which they think the body sway affects the acceleration obtained from head trajectories, while the effect is not considered in the social force model. Besides, the acceleration is sensitive to small noises of a trajectory. In our opinion, it is also a limitation of the model if it can only be used in the evaluating of the

force-based models. Hence in [27, 28], e is based on the position rather than the acceleration of pedestrians:

$$e = \sum_{i} \sum_{t=t_i^{start}}^{t_i^{end}} D(p_i(t), \tilde{p}_i(t))^2 / (t_i^{out} - t_i^{in}) / A, \tag{2}$$

where $p_i(t)$ is the measured position of pedestrian i at time t. $\tilde{p}_i(t)$ is the simulated position. The function $D()$ is to solve the distance between two points. Because of trajectories in the simulation and in the experiment are only synchronized when a pedestrian entering a scenario, e in this method will be sensitive to the direction discrepancy and the length of the trajectory. Imagining that if a small direction discrepancy happens at the beginning of the simulation, the error obtained by Eq. 2 will be amplified with the increasing of the trajectory length. This problem is improved in [29], in which the pedestrians in the simulation and in the experiment are synchronized every 1.5 s. Although the existing microscopic evaluating methods are able to optimize parameters of a model, there are some problems when applying them to evaluate a model. The main problem is that the errors in existing microscopic methods are one dimensional, from which we can only know the performance of a model is better or worse than another model. However, what results in the performance difference can not be speculated from the results described by numbers.

Besides, trajectory data used in existing microscopic estimation methods are singular: bidirectional trajectories in corridors [28] or several observation scenarios [27, 29]. Comprehensive evaluation in different densities and scenarios are still rare. In this paper, we evaluate a continuous model with a directional microscopic method. The method is proposed in Section 2. Based on the method a model introduced in Section 3 is evaluated in Section 4. At last, we discuss the results in Section 5.

2. Methods

To avoid the problems mentioned in Section 1, a generalized method is designed to include the following features:

(a) Independent of the used scenario,

(b) able to get rich information from one trajectory,

(c) insensitive to the length of trajectory,

(d) and the evaluated results have a directional physical meaning.

The original trajectory of a pedestrian i (j_i^{ori}) used in the method is the positions at continuous time steps:

$$j_i^{ori} = \{\boldsymbol{r}_{i,n}^{ori} | n = 0, 1, 2, ...\}, \tag{3}$$

where $\boldsymbol{r}_{i,n}^{ori}$ is the pedestrian position at the n-th time step. Extracting head positions from top-view videos could be the most common used method to obtain a trajectory. To reduce

the influence of the swing of the head, the trajectory should be smoothed before solving the velocity. The smoothing method and the velocity solving method are introduced in Appendix A. If the evaluation is conducted on each time step, the result of the model will be sensitive to small errors, especially the angular error defined in Eq. 5. So the trajectory is resmapled after smoothing. The resampling method is also introduced in Appendix A. Furthermore, an area selection technique is provided to conduct an evaluation in a specific area A. A point in j_i^{res} (a trajectory after the resampling) belongs to j_i^{slc} (the trajectory after the selection) if it is inside A:

$$j_i^{slc} = \{\boldsymbol{r}_{i,k}^{smt} | \boldsymbol{r}_{i,k}^{smt} \in A, k \in \{0, N, 2N, ...\}\}.^{1} \tag{4}$$

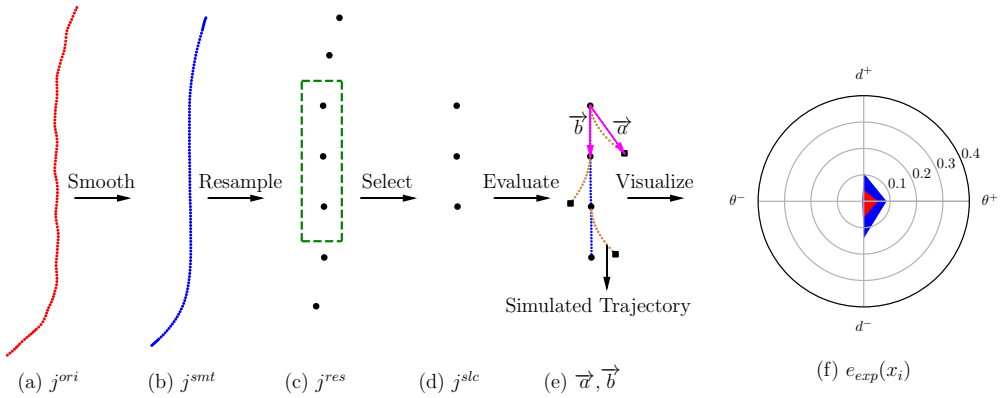

Fig. 1. The procedures of the trajectory processing and the evaluation.

The procedures of the trajectory processing are shown in Fig. 1 (a)-(d). In the following, we define the microscopic error by comparing trajectories in the simulation and in the experiment. At time step k in j_i^{slc}, all agents in the simulation have the same position and velocity with the pedestrians in the experiment. The movement of pedestrian i is simulated with a continuous model until $k+N$, while the other pedestrians are moved exactly as their smoothed trajectories in the experiment. The distance error d and the angular error θ are

$$\begin{aligned} d(k) &= (||\boldsymbol{a}|| - ||\boldsymbol{b}||)/D, \\ \theta(k) &= \arcsin\left(\frac{\boldsymbol{a} \times \boldsymbol{b}}{||\boldsymbol{a}||||\boldsymbol{b}||}\right)/\Theta, \\ \boldsymbol{a} &= \mathbf{r}_i^{sim}(k+N) - \mathbf{r}_i^{smt}(k), \\ \boldsymbol{b} &= \mathbf{r}_i^{smt}(k+N) - \mathbf{r}_i^{smt}(k), \end{aligned} \tag{5}$$

where $\mathbf{r}_i^{sim}(k)$ is the pedestrian position at the k-th time step in the simulation. $D = 1$ m and $\Theta = 1$ rad are the normalized parameters. According to the definition and Fig. 1 (e),

[1] $\boldsymbol{r}_{i,k}^{smt}$ is the k-th time step in the smoothed trajectory. N in the resampling interval. More details see Appendix A.

$\boldsymbol{a}$ is the motion vector of the pedestrian in the simulation, and $\boldsymbol{b}$ is the motion vector in the experiment. Therefore, when $d(k) > 0$, the mean speed in the simulation is larger than that in the experiment. When $\theta(k) > 0$, the direction of the velocity has a bias to right when comparing to that in the experiment. Based on d and θ, the error of the frame $e_{fra}(k)$ is

$$e_{fra}(k) = \{d^+(k), d^-(k), \theta^+(k), \theta^-(k)\}, \tag{6}$$

where $d^+ = ||d||$, $d^- = 0$ when $d \geq 0$. $d^+ = 0$, $d^- = ||d||$ when $d < 0$. θ^+ and θ^- are obtained with a similar manner. The four elements describe the error of the speed and the direction in positive and negative respectively. The error of the trajectory $e_{trj}(j_i)$ is

$$e_{trj}(j_i) = \{\mu_{d^+}(j_i), \mu_{d^-}(j_i), \mu_{\theta^+}(j_i), \mu_{\theta^-}(j_i)\}, \tag{7}$$

where $\mu_{d^+}(j_i) = \frac{1}{n_k}\sum d^+(k)$ is the mean value of all frames in the direction of d^+ (n_k is the number of frame in j_i^{slc}). $\mu_{d^-}(j_i)$, $\mu_{\theta^+}(j_i)$, and $\mu_{\theta^-}(j_i)$ can be solved analogically. According to the definition, $e_{trj}(j_i)$ describes the mean errors of a trajectory in the four directions. At last, the error of the experiment $e_{exp}(x_i)$ is

$$e_{exp}(x_i) = \{\{\mu_{d^+}(x_i), \sigma_{d^+}(x_i)\}, \{\mu_{d^-}(x_i), \sigma_{d^-}(x_i)\}, \{\mu_{\theta^+}(x_i), \sigma_{\theta^+}(x_i)\}, \{\mu_{\theta^-}(x_i), \sigma_{\theta^-}(x_i)\}. \tag{8}$$

Each item of $e_{exp}(x_i)$ is composed of the mean value and the standard deviation of all trajectories in the specific direction:

$$\begin{aligned} \mu_{d^+}(x_i) &= \frac{1}{n_j}\sum d^+(j_i), \\ \sigma_{d^+}(x_i) &= \sqrt{\frac{1}{n_j}\sum (\mu_{d^+}(j_i) - \mu_{d^+}(x_i))^2}, \end{aligned} \tag{9}$$

where n_j is the number of trajectories in the experiment. $e_{exp}(x_i)$ can be visualized with a radar chart (also referred as a error chart of an experiment). As shown in Fig. 1 (f), the vertex of inside polygon is the mean value. The vertex of the outside polygon is the sum of mean value and the standard deviation. Synthesizing the mean values, the standard deviations and the symmetry of the chart, the evaluation result can be described with a number $E(x_i)$:

$$E(x_i) = \exp\left(P(x_i) + S(x_i) + Y(x_i)\right), \tag{10}$$

where

$$P = \mu_{d^+} + \mu_{d^-} + \mu_{\theta^+} + \mu_{\theta^-}$$

is the sum of the mean values (referred as the precision of the model),

$$S = \sigma_{d^+} + \sigma_{d^-} + \sigma_{\theta^+} + \sigma_{\theta^-}$$

is the sum of the standard deviations (referred as the stability of the model), and

$$Y = \left(\frac{|(\mu_{d^+} + \sigma_{d^+}) - (\mu_{d^-} + \sigma_{d^-})|}{|(\mu_{d^+} + \sigma_{d^+}) + (\mu_{d^-} + \sigma_{d^-})|} + \frac{|(\mu_{\theta^+} + \sigma_{\theta^+}) - (\mu_{\theta^-} + \sigma_{\theta^-})|}{|(\mu_{\theta^+} + \sigma_{\theta^+}) + (\mu_{\theta^-} + \sigma_{\theta^-})|}\right)/2$$

is the symmetric factor of the outside polygon in the radar chart (referred as the symmetry of the model).

3. Materials

3.1. Specification of the Social Force Model

The circular specification of the social force model [29, 30] is selected to demonstrate the evaluation process of the method. In this model, velocity is calculated with an acceleration equation when no physical contact happens between pedestrians:

$$\frac{d\mathbf{v}_i}{dt} = \frac{v_i^0 \mathbf{e}_i - \mathbf{v}_i}{\tau_i} + \sum_{j(\neq i)} \boldsymbol{f}_{ij}(t) + \sum_w \boldsymbol{f}_{iw}(t). \tag{11}$$

The first term is the desire force, which describes the pedestrian is willing to move to a desire direction $\boldsymbol{e}_i$ with a desire speed v_i^0. $\boldsymbol{v}_i$ is the velocity. τ_i is the relaxation time (the time needed to accelerate to desire velocity). $\boldsymbol{f}_{ij}$ is the repulsive force between pedestrian i and pedestrian j:

$$\boldsymbol{f}_{ij}(t) = \sum_j A_i e^{(R_i + R_j - ||\mathbf{d}_{ij}||)/B_i} \frac{\mathbf{d}_{ij}}{||\mathbf{d}_{ij}||} \cdot w(\varphi_{ij}), \tag{12}$$

where $\mathbf{d}_{ij}$ is the vector point from j to i. R_i and R_j are the radius of the pedestrian. In our evaluation, $R = 0.25$ m. A_i reflects the strength of interaction, and B_i corresponds to the interaction range. $w(\varphi_{ij})$ is the anisotropy factor describing the different reactions of a pedestrian to what happens in front and behind:

$$w(\varphi_{ij}) = \lambda + (1 - \lambda)\frac{1 + \cos(\varphi_{ij})}{2}, \tag{13}$$

$$\cos(\varphi_{ij}) = \frac{\mathbf{v}_i}{||\mathbf{v}_i||} \cdot \frac{-\mathbf{d}_{ij}}{||\mathbf{d}_{ij}||}. \tag{14}$$

The repulsive force of wall has a similar form with Eq. (12):

$$\boldsymbol{f}_{wi}(t) = A_w e^{(R_i - ||\mathbf{d}_{iw}||)/B_w} \frac{\mathbf{d}_{iw}}{||\mathbf{d}_{iw}||}, \tag{15}$$

in which $\mathbf{d}_{iw}$ is the vector points from the pedestrian to the point on the wall which has the minimal distance to the pedestrian. Parameters listed in Table 1 are the calibration results of the evolutionary adjustment from three observation experiments [29]. P_1 is the calibration results without considering the anisotropy ($\lambda = 1$), and P_2 is the optimal parameters with an appropriate anisotropy factor ($\lambda = 0.12$). Note that in [30], the parameters of the repulsive forces of the wall and the pedestrians are not distinguished. So A_w and B_w are the same with A_i and B_i in P_1 and P_2. P_3 is the adjusting result of this paper.

Table 1: Parameter sets in Ref. [29] and in this paper.

Parameters	A_w	B_w	A_i	B_i	λ	τ
P_1	0.11	0.84	0.11	0.84	1	0.5
P_2	0.42	1.65	0.42	1.65	0.12	0.5
P_3	0.80	0.30	0.42	1.25	0.12	0.5

3.2. Trajectory Database

Trajectories used in the evaluation come from PED Data Archive [2], which are extracted automatically from video recordings of controlled experiments by using the software PeTrack [31]. Experiments of unidirectional, bottleneck, bidirectional scenarios are involved in the evaluation. Sketches of these scenarios are shown in Fig. 2, in which pedestrians start from the waiting area (blue rectangle in Fig. 2), then cross the corridor with an expected exit (red dashed line in Fig. 2). Density in the corridor is controlled by the width of entrance b_{in} and the number of pedestrians in the waiting area.

All participants walk from the left to the right to cross the corridor in unidirectional and bottleneck experiments(more details of the experiments can be found in [32]). In bidirectional experiments, participants are asked to leave the corridor by left or right side according to a number given to them in advance. We simulate the process by setting four virtual exits. As shown in Fig. 2 (c), the width of each exit is 1/3 of the total width. The desire exit is assigned the one which is more close to the pedestrian when he or she leaves the corridor. More information about the bidirectional experiments can be found in [33]. To reduce the influence of the entrance and the exit, investigation areas are selected as the middle part in the corridor (yellow areas in Fig. 2). Parameters of the experiments are shown in Table 2. According to [32, 33], the desire speed is $v_0 = 1.5$ m/s in the experiments.

Table 2: Experiment parameters. In bidirectional experiments, the two numbers of "Participant number" are the pedestrians in the left and right waiting area respectively. $\overline{\rho}$ is the mean density in the investigation area.

Scenario	Experiment	Participant number	b_{in}(m)	b_{exit}(m)	$\overline{\rho}$(ped/m^2 or m)
Unidirectional	U_1	61	0.50	-	0.40
	U_2	66	0.60	-	0.46
	U_3	111	0.70	-	0.57
	U_4	121	1.00	-	0.93
	U_5	175	1.45	-	1.30
	U_6	220	1.80	-	1.38
Bottleneck	T_1	170	1.80	1.20	1.63
	T_2	159	1.80	0.95	1.93
	T_3	148	1.80	0.70	2.24
Bidirectional	B_1	54/71	0.50	-	0.42
	B_2	61/86	0.75	-	0.65
	B_3	119/97	0.85	-	0.97
	B_4	125/105	1.00	-	1.33

[2] http://ped.fz-juelich.de/db

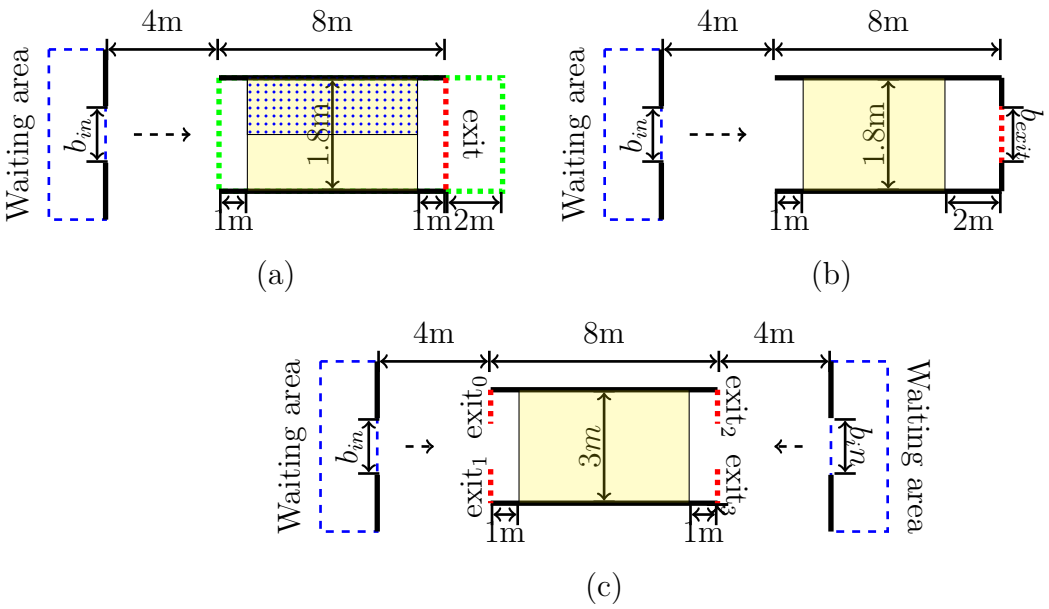

Fig. 2. Sketch of experiments in different scenarios. (a) Unidirectional scenario. (b) Bottleneck scenario. (c) Bidirectional scenario.

4. Results

4.1. microscopic evaluation in unidirectional scenario

By observing the error charts of the parameter set P_1, we find that the speed in the simulation is much larger than that in the experiment, especially in high density situations. The radar chart of $e_{exp}(U_5)$ with P_1 is shown in Fig. 3(a), in which the simulated speed is much larger than the actual speed in experiment. The possible reason could be that the repulsive force between pedestrians is too weak. We adjust the force by increasing A_i to 0.50. However, according to Fig. 3(b), the symmetry has no improvement while the stability becomes even worse. The reason should be that when $\lambda = 1$, repulsive forces from front and back pedestrians are similar in most cases when the pedestrian is walking in the controlled experiments. The forces will be counteracted by each other along the walking direction. Further increasing A_i does not slow down the pedestrian. While after considering the anisotropy ($\lambda = 0.12$), the speed becomes smaller (see Fig. 3(C)), and there is a significant improvement of the symmetry. In summary, a systematic error (bias to d^+) will be caused when using isotropous repulsive force between pedestrians.

The error chart of $e_{exp}(U_5)$ with P_2 is shown in Fig. 3 (d). Compared to the Fig. 3 (c), the speed becomes smaller, while the error of direction (θ^+ and θ^-) becomes larger. Considering the strength factor A_i in Fig. 3 (c) is smaller than that in Fig. 3 (d), but the speed is much slower, we suspect that the effective range factor B_i is too large in P_2, since with a large B_i, more neighbors will have significant influence to the pedestrian. Sequentially, the speed will be smaller. If a pedestrian is close to the wall, the crowd around her will be asymmetric. As a result, the direction error (θ^+ and θ^-) will be large in such a case.

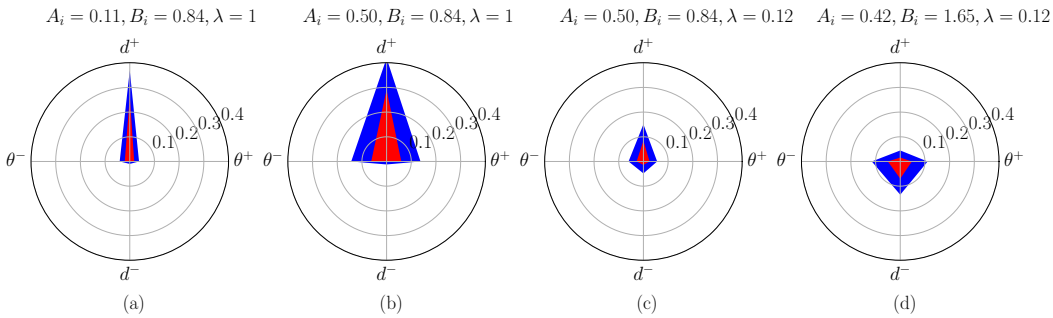

Fig. 3. Radar chart of $e_{exp}(U_5)$ with different A_i, B_i and λ

Furthermore, the performance of the wall repulsive force (Eq. 15) can be evaluated with the error chart of the dot area in Fig. 2(a), which is the upper half of the yellow area. According to Fig. 4, the simulated trajectories drift away from the wall in low density, while drift toward the wall in high density. It means that the repulsive force is too strong in low density and too weak in high density. This is due to the fact that a wall acts like a static pedestrian, if the repulsive forces of wall-pedestrians and pedestrian-pedestrian have the same strength parameter. In low density, there are less lateral agents around the pedestrian. In addition to the anisotropy is not considered in Eq. 15, the lateral force exerted by the wall will be larger than the repulsive force of pedestrians in most cases. In high density, however, the lateral force of pedestrians increases significantly while the force of wall remains unchanged. We think this problem can be improved by increasing A_w and decreasing B_w to obtain a stronger wall repulsive force near the wall, and a weaker wall repulsive force far from the wall.

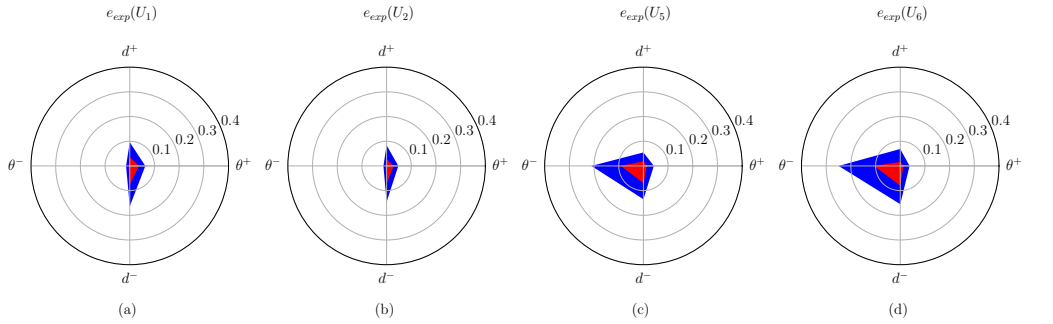

Fig. 4. Evaluations of dot area in unidirectional experiments.

In summary, three conclusions are obtained with the microscopic evaluation:

(1) The simulated speed is too large in high density situations with P_1.

(2) The simulated speed is too small in high density situations with P_2.

(3) The pedestrians are too close to the wall in high density situations with P_2.

4.2. macroscopic verification in unidirectional scenario

To verify the conclusions in Sec. 4.1, we simulate the movements of all pedestrian with the following rules:

(a) Pedestrians move as in the experiments before they enter the simulation field.

(b) Pedestrians are driven by the model when they are in the simulation field.

(c) Pedestrians are removed when they are outside the simulation field.

The simulation field of the unidirectional scenario is the green box in Fig. 2 (a). In experiments, pedestrians still move to leave the scenario after they walk out of the corridor. Hence, simulation field is two meters longer than the corridor. Then we can make a comparison with some macroscopic features. At first, the trajectories of U_6 in the experiment and the simulations are shown in Fig 5. For clarity, ten percent of trajectories are displayed.

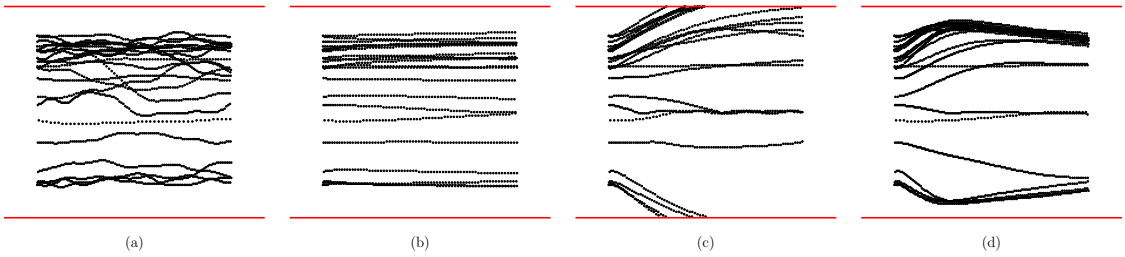

Fig. 5. Experimental and simulated trajectories of U_6. (a) Experimental trajectories. (b) Simulated with P_1. (c) Simulated with P_2. (d) Simulated with $A_w = 0.80$, $B_w = 0.30$.

As shown in Fig. 5 (c), some trajectories near the wall intersect with the wall. It indicates that the wall repulsive force is too small with P_2 and some pedestrians are pushed outside the wall in high density. Therefore, conclusion (3) is correct.

Then we verify the conclusions (1) and (2) by comparing the mean speed. According to Fig. 6 (a), the mean speed of all pedestrians in the simulation with P_1 is close to the free speed 1.5 m/s in the whole simulation. While in the experiment, the speed decreases clearly with more pedestrians entering the investigation area. It indicates that the isotropous social force between pedestrians is unable to slow down the pedestrians in U_6. Therefore, conclusion (1) is correct.

However, according to Fig. 6 (a), in most time steps the mean speed with P_2 is also larger than that in the experiment, rather than smaller as shown in Fig. 3 (d). We think the main reason is that in the simulation of the macroscopic evaluation, some pedestrians are removed when they cross the wall, so that it is irrational to verify conclusion (2) by comparing the speed of the crowd directly. Considering no pedestrian crosses the wall with

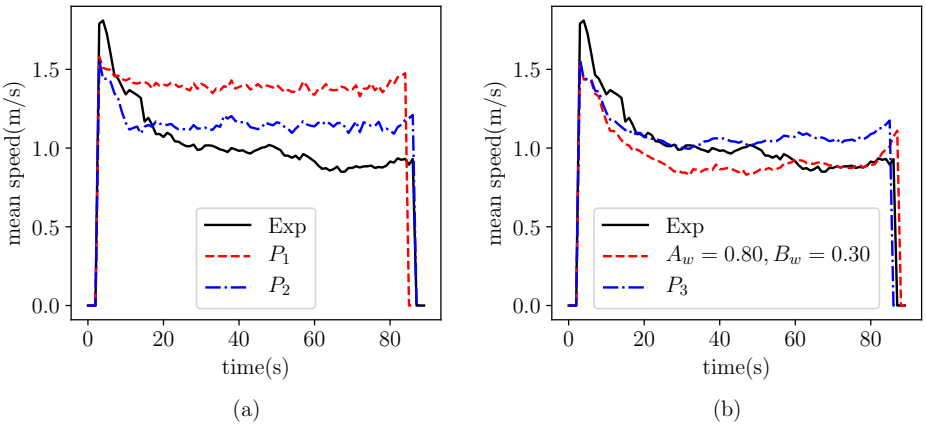

Fig. 6. The comparison of the speed in the experiment and the simulations.

P_1 (see Fig. 5 (a)), we think that conclusion (1) still holds. Hence, the wall repulsive force should be adjusted first before verifying conclusion (2).

According to the fact mentioned in Sec. 4.1, A_w should be increased and B_w should be decreased. The trajectories simulated with $A_w = 0.80$, $B_w = 0.30$ (the other parameters are the same with the values in P_2) are shown in Fig. 5 (d), in which all pedestrians move inside the investigation area. Then we compare the mean speed in Fig. 6 (b). In most time steps, the speed in the simulation is smaller than that in the experiment. The conclusion (2) is verified. Furthermore, we follow the fact mentioned in Sec. 4.1 to decrease B_i in P_2. The error chart with $B_i = 1.25$ is shown in Fig. 7. Both the inner polygon and the outer polygon are small and symmetrical. As it is shown in Fig. 6 (b), the macroscopic parameter (mean speed) also shows a good agreement with the experiment.

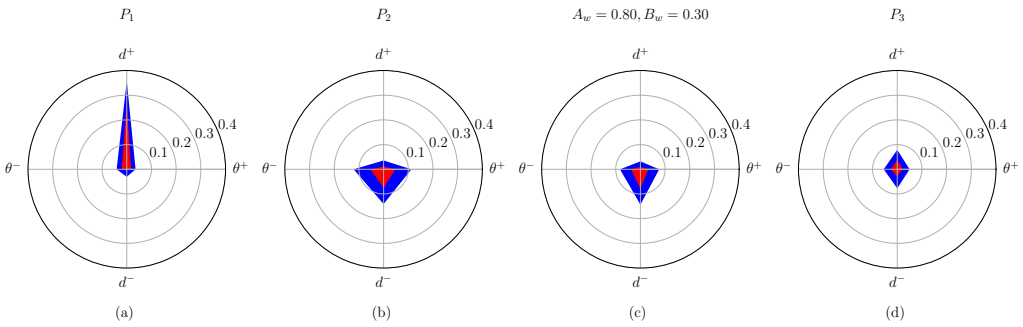

Fig. 7. The error charts of $e_{exp}(U_6)$ with different parameter sets.

In summary, all of the three conclusions deduced from the error charts of the microscopic evaluation method are verified by the macroscopic comparisons. The directions of the bias in the error charts have good agreements with the macroscopic evaluations. Most of all, according to Fig. 6 and 7, a parameter set with a smaller error at the microscopic level

always has a better performance at the macroscopic level.

4.3. Quantitative results of the microscopic evaluation

Evaluating all experiments with the microscopic method, we get a comprehensive and quantitative assessment of the investigated model. The evaluation results of P_2 and P_3 are shown in Table. 3. From the table we can see that from P_2 to P_3, the improvement is significant in unidirectional and bidirectional experiments, especially in high density situations. While the improvement is not significant in bottleneck experiments. When focusing on P_2 and P_3 respectively, we find that P_2 has a better performance in low density, unidirectional and bottle neck scenarios. P_3 has a better performance in high density, unidirectional and bidirectional scenarios. This implies the parameter are "optimal" only with respect to a specific scenario and density . If a threshold ($E = 1.55$) is set for the applicability, we can obtain a quantitative description of P_3. Based on the evaluation results of trajectories database of this paper, P_3 is applicable in unidirectional scenario with a mean density ranges from 0.93 to 1.38 ped/m^2. However, the threshold may be different when applying the model to different scenarios.

Table 3: Quantitative evaluation results of P_2 and P_3.

x_i	$\exp(P(x_i))$		$\exp(S(x_i))$		$\exp(Y(x_i))$		$E(x_i)$	
	P_2	P_3	P_2	P_3	P_2	P_3	P_2	P_3
U_1	1.18	1.16	1.22	1.21	1.25	1.21	1.80	1.70
U_2	1.16	1.15	1.19	1.20	1.31	1.20	1.81	1.70
U_3	1.12	1.23	1.18	1.17	1.37	1.20	1.85	1.58
U_4	1.17	1.11	1.16	1.14	1.48	1.23	2.01	1.55
U_5	1.20	1.13	1.25	1.16	1.37	1.11	1.95	1.46
U_6	1.21	1.12	1.25	1.16	1.37	1.03	2.07	1.34
T_1	1.30	1.22	1.40	1.25	1.08	1.22	1.96	1.87
T_2	1.41	1.33	1.51	1.29	1.22	1.45	2.59	2.51
T_3	1.54	1.36	1.71	1.42	1.05	1.18	2.77	2.29
B_1	1.23	1.18	1.18	1.17	1.62	1.55	2.36	2.14
B_2	1.22	1.14	1.27	1.15	1.46	1.39	2.37	1.81
B_3	1.22	1.16	1.27	1.19	1.46	1.14	2.37	1.58
B_4	1.40	1.22	1.41	1.26	1.66	1.19	3.28	1.83

5. Conclusion

In this paper, we propose a microscopic method to evaluate a continuous model by means of the trajectories. The microscopic error of a trajectory is defined in four directions, which corresponds to the positive and the negative deviations of the speed and the direction respectively. The microscopic error of an experiment, which can be visualized by a radar chart, is then defined as the mean values and standard deviations of all trajectories in the experiment. Qualitative conclusions can be deduced from the radar chart. Synthesizing the vertex values and the shape of the radar chart, the evaluation result is finally described by a quantitative value.

With the microscopic method, a social force model is evaluated with 1,936 trajectories in three different scenarios. Based on the error charts of unidirectional experiments, three qualitative conclusions are summarized. Some suggestions on how to modify the parameters are also made from the error charts. In the following we verify the conclusions with the macroscopic level comparison. The verification results show that all conclusions deduced from the microscopic method are reasonable. Most of all, a parameter set with smaller error in the microscopic evaluation always has a better performance at the macroscopic level. Finally, we discuss the possible quantitative descriptions of a model with the microscopic method.

The method is defined at the trajectory level, therefore its effectiveness is the same in different scenarios. The evaluation is conducted many times along one trajectory, hence, we can get rich information from one trajectory. Because of the simulation and the experiment is synchronized at the beginning of each evaluation, the result is insensitive to the length of a trajectory. The result has four directions, based on which qualitative conclusions can be obtained from the trajectory level comparison. Moreover, the final result E is a comprehensive evaluation of the precision, the stability and the symmetry of a model.

We suggest that the microscopic method and the trajectory database can be used as a standard criterion to give qualitative and quantitative evaluations of a model. In the future, we will try to establish an evaluation database of continuous pedestrian dynamic models based on the method. The database will be composed of experimental trajectories with graded densities and various scenarios, and evaluations results of different models with these trajectories.

A. Appendix A: Methods of the trajectory smoothing, resampling and the velocity solving

A trajectory is smoothed by averaging the positions of adjacent time steps:

$$j_i^{smt} = \{\boldsymbol{r}_{i,n}^{smt} | \boldsymbol{r}_{i,n}^{smt} = \frac{1}{K_1} \sum_{n-K_1/2}^{n+K_1/2} \boldsymbol{r}_{i,n}^{ori}, n = 0, 1, 2, ...\}, \tag{16}$$

where K_1 is the number of the time step for the smoothing. The sampling result of the trajectory i is:

$$j_i^{res} = \{\boldsymbol{r}_{i,n}^{smt} | n = 0, N, 2N, ...\}, \tag{17}$$

where N is the interval between two resamplings. The velocity of a time step ($v(n)$) depends on the future movement of the pedestrian:

$$\boldsymbol{v}_i(n) = \frac{\boldsymbol{r}_{i,n+K_2}^{smt} - \boldsymbol{r}_{i,n}^{smt}}{K_2 \delta}, \tag{18}$$

where δ is the duration of the time step in the original trajectory.

In this paper, $K_1 = N = K_2 = 1/\delta$. It means that all of the intervals (the smooth interval, the resampling interval and the velocity solving interval) are 1 s.

Acknowledgement

This research was supported by Key Research and Development Program (2018YFC0807000), Fundamental Research Funds for the Central Universities (WK2320000036), Program of Shanghai Science and Technology Committee (19QC1400900), and the State Key Laboratory of Fire Science in University of Science and Technology of China (No. HZ2018-KF12).

References

[1] S. Okazaki, A study of pedestrian movement in architectural space, part 1: Pedestrian movement by the application on of magnetic models, Trans. AIJ 283 (1979) 111–119.

[2] T. Korhonen, S. Hostikka, O. Keski-Rahkonen, A proposal for the goals and new techniques of modelling pedestrian evacuation in fires, Fire Safety Science 8 (2005) 557–567.

[3] S. Cao, L. Fu, P. Wang, G. Zeng, W. Song, Experimental and modeling study on evacuation under good and limited visibility in a supermarket, Fire Safety Journal 102 (2018) 27–36.

[4] B. Jiang, Simped: simulating pedestrian flows in a virtual urban environment, Journal of geographic information and decision analysis 3 (1) (1999) 21–30.

[5] W. Shao, D. Terzopoulos, Autonomous pedestrians, in: Proceedings of the 2005 ACM SIGGRAPH/Eurographics symposium on Computer animation, ACM, 2005, pp. 19–28.

[6] J. Ma, W.-g. Song, J. Zhang, S.-m. Lo, G.-x. Liao, k-nearest-neighbor interaction induced self-organized pedestrian counter flow, Physica A: Statistical Mechanics and its Applications 389 (10) (2010) 2101–2117.

[7] W. Song, X. Xu, B.-H. Wang, S. Ni, Simulation of evacuation processes using a multi-grid model for pedestrian dynamics, Physica A: Statistical Mechanics and its Applications 363 (2) (2006) 492–500.

[8] S. Cao, W. Song, W. Lv, Z. Fang, A multi-grid model for pedestrian evacuation in a room without visibility, Physica A: Statistical Mechanics and its Applications 436 (2015) 45–61.

[9] D. Helbing, P. Molnar, Social force model for pedestrian dynamics, Physical review E 51 (5) (1995) 4282.

[10] W. Yu, R. Chen, L. Dong, S. Dai, Centrifugal force model for pedestrian dynamics, Physical Review E 72 (2) (2005) 026112.

[11] M. Chraibi, A. Seyfried, A. Schadschneider, Generalized centrifugal-force model for pedestrian dynamics, Physical Review E 82 (4) (2010) 046111.

[12] A. Tordeux, M. Chraibi, A. Seyfried, Collision-free speed model for pedestrian dynamics, in: Traffic and Granular Flow'15, Springer, 2016, pp. 225–232.

[13] F. Chittaro, F. Jean, P. Mason, On the inverse optimal control problems of the human locomotion: stability and robustness of the minimizers, Journal of Mathematical Sciences 195 (3) (2013) 269–287.

[14] A. V. Papadopoulos, L. Bascetta, G. Ferretti, A comparative evaluation of human motion planning policies, IFAC Proceedings Volumes 47 (3) (2014) 12299–12304.

[15] G. Arechavaleta, J.-P. Laumond, H. Hicheur, A. Berthoz, Optimizing principles underlying the shape of trajectories in goal oriented locomotion for humans, in: Humanoid Robots, 2006 6th IEEE-RAS International Conference on, IEEE, 2006, pp. 131–136.

[16] M. J. Seitz, G. Köster, Natural discretization of pedestrian movement in continuous space, Physical Review E 86 (4) (2012) 046108.

[17] I. von Sivers, G. Köster, Dynamic stride length adaptation according to utility and personal space, Transportation Research Part B: Methodological 74 (2015) 104–117.

[18] S. Heliövaara, T. Korhonen, S. Hostikka, H. Ehtamo, Counterflow model for agent-based simulation of crowd dynamics, Building and Environment 48 (2012) 89–100.

[19] D. R. Parisi, M. Gilman, H. Moldovan, A modification of the social force model can reproduce experimental data of pedestrian flows in normal conditions, Physica A: Statistical Mechanics and its Applications 388 (17) (2009) 3600–3608.

[20] T. I. Lakoba, D. J. Kaup, N. M. Finkelstein, Modifications of the helbing-molnar-farkas-vicsek social force model for pedestrian evolution, Simulation 81 (5) (2005) 339–352.
[21] W. Liao, J. Zhang, X. Zheng, Y. Zhao, A generalized validation procedure for pedestrian models, Simulation Modelling Practice and Theory 77 (2017) 20 – 31.
[22] A. Seyfried, M. Boltes, J. Kähler, W. Klingsch, A. Portz, T. Rupprecht, A. Schadschneider, B. Steffen, A. Winkens, Enhanced empirical data for the fundamental diagram and the flow through bottlenecks, in: Pedestrian and Evacuation Dynamics 2008, Springer, 2010, pp. 145–156.
[23] U. Weidmann, Transporttechnik der fussgänger, Schriftenreihe/Institut für Verkehrsplanung, Transporttechnik, Strassen-und Eisenbahnbau 90 (1992).
[24] H. Benner, J. Lohmiller, P. Sukennik, Is calibration a straight-forward task if detailed trajectory data is available?, Tech. rep. (2017).
[25] S. Seer, C. Rudloff, T. Matyus, N. Brändle, Validating social force based models with comprehensive real world motion data, Transportation Research Procedia 2 (2014) 724–732.
[26] S. P. Hoogendoorn, W. Daamen, Microscopic parameter identification of pedestrian models and its implications to pedestrian flow modeling, Transporttation Research Board Annual Meeting, 2006.
[27] C. Rudloff, T. Matyus, S. Seer, D. Bauer, Can walking behavior be predicted? analysis of calibration and fit of pedestrian models, Transportation Research Record: Journal of the Transportation Research Board (2264) (2011) 101–109.
[28] S. Seer, N. Brändle, C. Ratti, Kinects and human kinetics: A new approach for studying pedestrian behavior, Transportation research part C: emerging technologies 48 (2014) 212–228.
[29] A. Johansson, D. Helbing, P. K. Shukla, Specification of the social force pedestrian model by evolutionary adjustment to video tracking data, Advances in complex systems 10 (supp02) (2007) 271–288.
[30] D. Helbing, A. Johansson, Pedestrian, crowd and evacuation dynamics, in: Encyclopedia of complexity and systems science, Springer, 2009, pp. 6476–6495.
[31] M. Boltes, A. Seyfried, B. Steffen, A. Schadschneider, Automatic extraction of pedestrian trajectories from video recordings, in: Pedestrian and Evacuation Dynamics 2008, Springer, 2010, pp. 43–54.
[32] J. Zhang, W. Klingsch, A. Schadschneider, A. Seyfried, Transitions in pedestrian fundamental diagrams of straight corridors and t-junctions, Journal of Statistical Mechanics: Theory and Experiment 2011 (06) (2011) P06004.
[33] J. Zhang, W. Klingsch, A. Schadschneider, A. Seyfried, Ordering in bidirectional pedestrian flows and its influence on the fundamental diagram, Journal of Statistical Mechanics: Theory and Experiment 2012 (02) (2012) P02002.